



**Amperometric hydrogen peroxide and glucose biosensor
based on the NiFe₂/ordered mesoporous carbon
nanocomposites**

Journal:	<i>Analyst</i>
Manuscript ID:	AN-ART-08-2014-001549.R1
Article Type:	Paper
Date Submitted by the Author:	10-Oct-2014
Complete List of Authors:	Xiang, Dong; Shandong Jianzhu University, ; Shandong University, School of Materials Science and Engineering Yin, Long-Wei; Shandong University, School of Materials Science and Engineering Ma, Jingyun; Shandong University, School of Materials Science and Engineering Guo, Enyan; Shandong University, School of Materials Science and Engineering Li, Qun; Shandong University, School of Materials Science and Engineering Li, Zhaoqiang; Shandong University, School of Materials Science and Engineering Liu, Kegao; Shandong Jianzhu University,

Amperometric hydrogen peroxide and glucose biosensor based on the NiFe₂/ordered mesoporous carbon nanocomposites

Dong Xiang^{a,b,*}, Longwei Yin^{b,*}, Jingyun Ma^b, Enyan Guo^b, Qun Li^b, Zhaoqiang Li^b, Kegao Liu^a

^a School of Material Science and Engineering, Shandong Jianzhu University, Jinan 250101, P. R. China. E-mail:

xiang@sdjzu.edu.cn; Tel.: + 86 531 86367285.

^b Key Laboratory of Liquid-Solid Structural Evolution and Processing of Materials, Ministry of Education, School of Materials Science and Engineering, Shandong University, Jinan 250061, P. R. China. E-mail:

yinlw@sdu.edu.cn; Tel.: + 86 531 88396970; Fax: + 86 531 88396970.

ABSTRACT: The nanocomposites of NiFe_x embedded ordered mesoporous carbon (OMC) ($x=0, 1, 2$) prepared by wet impregnation and hydrogen reduction process were used to construct electrochemical biosensor for the amperometric detection of hydrogen peroxide (H₂O₂) or glucose. NiFe₂/OMC nanocomposites are demonstrated with a large surface area, suitable mesoporous channels, many edge-plane-like defective sites, and good distributed of alloyed nanoparticles. NiFe₂/OMC and Nafion modified glass carbon electrode (GCE) exhibited excellent electrocatalytic activities toward the reduction of H₂O₂ as well. By utilizing it as bioplatfrom, GOx (glucose oxidase) cross-linked with Nafion was immobilized on the surface of the electrode for the construction of the amperometric glucose biosensor. Our results indicated that the amperometric hydrogen peroxide biosensor (NiFe₂/OMC+Nafion+GCE) showed good analytical performances in term of a high sensitivity of 4.29 $\mu\text{A mM}^{-1} \text{cm}^{-2}$, wide linearity from 6.2 to 42710 μM and low detection limit of 0.24 μM at a signal-to-noise ratio of 3 ($S/N=3$). This biosensor possessed of an excellent selectivity, high stability and negligible interference for detection of H₂O₂. In addition, the immobilized enzyme on NiFe₂/OMC+Nafion+GCE, retaining its bioactivity, exhibited a reversible two-proton and two-electron transfer reaction, fast heterogeneous electron transfer rate and an effective Michaelis–Menten constant (K'_M) (3.18 mM). GOx+NiFe₂/OMC+Nafion+GCE could be used to detect of glucose based on the oxidation of glucose catalyzed by GOx and exhibited a wide detection range of 48.6-12500 μM with high sensitivity of 6.9 $\mu\text{A mM}^{-1} \text{cm}^{-2}$ and low detection limit of 2.7 μM ($S/N=3$). The enzymic biosensor maintained a high selectivity and stability features, which had a great promising application for detection of glucose.

Introduction

The application of biosensors to the detection of biomolecule at low concentration plays a crucial role in early diagnosis and cure of diseases.^{1,2} Hydrogen peroxide (H_2O_2) is a material used as an oxidizing agent in biological and chemical industries.³ It is an important intermediate oxidation products of glucose catalyzed by glucose oxidase (GOx) in the presence of O_2 where the detection of pathological in various diseases can be achieved. Glucose is a metabolite for living organisms, especially in the case of patients suffering from diabetes.^{4,5} Among the methods for detecting H_2O_2 and glucose⁶⁻⁸, the electrochemical method has been proved to be attractive because of its convenience, low cost, high selectivity, and high sensitivity.^{9,10} Particularly, the high selectivity and sensitivity of glucose enzymatic (glucose oxidase, GOx) biosensors have been widely used in practical detecting process because of their vital role in blood glucose monitoring in diabetic patients.^{1,11} However, some properties, including chemical and thermal instabilities, can change the activity of enzymes to cause degeneration, low activity and less reproducibility¹². Detection of H_2O_2 is confronted with the same problem. The growing emergence of nanomaterials provides the prerequisites for developing electrochemical biosensor in the direction of high sensitivity, timely and accurate detection due to their extremely reduced sizes, large surface-to-volume ratio, high level of crystallinity.^{1,10} To address this challenge, amperometric electrochemical biosensor of composite nanomaterials with carbon is the significant focus of this research.

Carbon materials have many electrochemical advantages, such as low background current, wide potential window, inert, low cost and high conductivity.¹³ Those are considered as good analysis and electrochemical performance of electrode materials. Carbon materials used in electrochemical biosensors mainly include graphite¹⁴, glassy carbon¹⁵, carbon fibers¹⁶, and carbon nanotubes^{17,18}. Ordered mesoporous carbon (OMC) is synthesized by the “template” method, where the ordered hexagonal and cubic mesoporous silicon or aluminum silicon can be used as an “inorganic template”.¹⁹ Especially, mesoporous carbon with orderly structure has been developed for catalytic applications, sensor, bioreactor and energy storage, etc.²⁰⁻²⁷ because of its excellent properties such as high specific surface area, tunable pore size distribution, high thermal stability, flexible structure, and electrical conductivity.²⁸⁻³¹ When OMC is used as modified electrode, it can conduct electron transfer between the substrates. Jia et al.³² reported that OMC modified electrode could be used to select and detect dopamine by ascorbic acid (AA) due to the catalytic oxidation properties. Zhou et al.³³ found that OMC had a higher and more stable electric catalytic response for NADH (Nicotinamide Adenine Dinucleotide Health) than carbon nanotubes' (CNTs). OMC can provide a platform of dehydrogenase-based electrochemical biosensors, which is benefit for the electronic conduction and results in good running of the electrochemical biosensor conducting. Zhou et al.²⁴ thought that OMC was the intrinsically conductive conductor which could play an important role in electron transfer with most of its redox partners. By means of high special surface area, OMC is

1 used as catalyst support to make electrochemical biosensor. Meanwhile, as active site, metal or metallic oxide
2 nanoparticles are embedded OMC, such as Pt^{34,35}, Au³⁶, Ag³⁷, Ni^{38,39}, Cu⁴⁰, CoO⁴¹, and so on. Yu et al.⁴² reported
3 that the glucose biosensor with high sensitivity was made from GOx immobilized a film of Pt nanoparticles
4 deposited mesoporous carbon (CMK-3) electrode. Ndamanisha et al.⁴³ demonstrated the ferrocene and
5 mesoporous carbon composite (OMC-Fe) was used to make H₂O₂ electrochemical sensor with high sensitivity and
6 stability. Compared with pure OMC, the detection range of OMC-Fe electrode for H₂O₂ increased, and had a good
7 reproducibility. In recent years, the application of monometallic electrode materials has two fundamental problems
8 including low efficiency and poisoning effect due to chemisorbed intermediates⁴⁴. Hence, nanocomposites
9 especially metallic alloy nanoparticles (MANPs) (such as Pt-Pd, Pt-Ir, Cu-Pd, Au-Pt, and Au-Ag)⁴⁵⁻⁴⁹ draw more
10 and more attentions for their potential applications in biotechnology and bioanalytical chemistry.^{50,51} MANPs
11 modified electrodes show outstanding advantages in electroanalysis such as catalysis, enhancement of mass
12 transport, good cooperated synergy, high effective surface area, and control over electrode microenvironment.^{52,53}
13 They often exhibit better catalytic properties than their monometallic counterparts.^{48,51,54} Pandey et al.⁵⁵
14 synthesized composite materials of PB–Au(I)/AuNPs–Pd for detection of H₂O₂ which exhibited excellent
15 electrocatalytic behavior as well as extended the applied potential of H₂O₂ reduction towards anodic direction.
16 Noh et al.⁵⁶ were the first to report catalysts for the oxidation of glucose and the reduction of H₂O₂ by using a
17 Cu–Co alloy dendrite, and the glucose sensor developed by them was successfully applied to a real human blood
18 sample analysis. The Cu–Co dendrite material can be widely used as a long-term stable catalyst for glucose and
19 H₂O₂ sensors.

20 Herein, NiFe_x/OMC nanocomposites were prepared by wet impregnation and hydrogen reduction method. The
21 electrochemical biosensor electrodes were fabricated by NiFe_x/OMC, Nafion, and glucose oxidase (GOx)
22 modified glass carbon electrode (GCE), including NiFe_x/OMC+Nafion+GCE and GOx+NiFe_x/OMC+Nafion
23 +GCE, respectively. The electrochemical performance of NiFe_x/OMC+Nafion+GCE was detected in H₂O₂ and
24 phosphate buffer solution (PBS), while GOx+NiFe_x/OMC+ Nafion+GCE was detected in glucose solution and
25 PBS. After successive addition H₂O₂ solution in PBS, the electrode showed a high sensitivity, low limit of
26 detection and wide linear detection range, but it was failed after addition of glucose solution. When GOx was
27 immobilized on the surface of GCE, GOx+NiFe_x/OMC+Nafion+GCE can keep high electrochemical performance
28 and stability in the detection of glucose in PBS under the action of the enzyme.

29 Experimental

30 Chemical and reagents

1
2
3
4
5
6
7
8
9
10
11
12
13
14
15
16
17
18
19
20
21
22
23
24
25
26
27
28
29
30
31
32
33
34
35
36
37
38
39
40
41
42
43
44
45
46
47
48
49
50
51
52
53
54
55
56
57
58
59
60

P123 triblock copolymer, Nafion-115[®] ion-crosslinked polymer, glucose oxidase (GOx, Type X-S, 100,000 U g⁻¹), and bovine serum protein were purchased from Aldrich, DuPont, Sigma, and JieRun (China), respectively. Phosphate buffer saline (0.1 M PBS) with 9 g/L NaCl at the different pH value was prepared from stock solutions of H₃PO₄, Na₂HPO₄, and NaH₂PO₄, which was used as the supporting electrolyte. The others chemicals such as Tetraethoxysilane (TEOS), sucrose, sulfuric acid (98%), hydrofluoric acid (HF, 40%), nickel acetate, iron nitrate, ethanol, hydrogen peroxide (H₂O₂, 37%), uric acid (UA, 99%), ascorbic acid (AA, 99.5%) and glucose were obtained from Sinopharm Chemical Reagent Co. Ltd. (China). Glucose stock solution was stored overnight at room temperature before measurement. The stock GOx solution was prepared in the PBS buffer and stored at 277 K. Unless otherwise stated, reagents were of analytical grade and used as received. Doubly distilled water was used throughout the whole experiments from a millipore system (>18 MΩ cm).

Apparatus and procedures

The structure, phase composition, and morphology of the as-prepared samples were investigated by X-ray diffraction (XRD, Rigaku D/max-2500, Cu K_α radiation) and transmission electron microscope (HR-TEM, JEM-2100). Nitrogen adsorption-desorption isotherms were determined at 77 K by using an adsorption porosimeter Micromeritics ASAP 2020 system. The surface area measurements were performed according to the Brunauer-Emmett-Teller (BET) method, while the pore size distribution was obtained from the adsorption branch of isotherm by using the corrected form of Kelvin equation by means of the Barrette Joynere Halenda (BJH) method. Raman spectrum was recorded by using a Horiba Jobin-Yvon microraman spectrometer, equipped with a microscope and a 633 nm laser as the excitation source.

Electrochemical performance conducted on a Princeton Parstate 2273A electrochemical station with a three-electrode system by using a Pt sheet as the counter electrode and an Ag/AgCl (in saturated KCl) as the reference electrode in PBS as the electrolyte. The preparation process of the working electrode was described in the latter of the sample preparation. The geometric surface area of the prepared working electrode was about 0.071 cm². The electrochemical impedance spectroscopy (EIS) measurements of the samples were performed under 0 V vs. open circuit potential with an excitation signal of 5 mV in the frequency range of 10 kHz~100 mHz in 0.1 M PBS solution containing 1.0 mM H₂O₂ or 1.0 mM glucose. The impedance data were fitted to an appropriate equivalent circuit using ZSimpWin 3.0 software (Echem Software). The cyclic voltammogram (CV) curves were recorded by electrochemical station in a potential range from -1.0 to 0.5 V with different scanning rates, and amperometric measurements were also recorded by magnetic stirring in PBS solution.

Preparation of SBA-15, OMC, and NiFe_x/OMC

In the present work, hexagonally ordered SBA-15 was used as a template for the synthesis of ordered mesoporous

1 carbon (OMC). The synthesis of SBA-15 was performed with the following method as: P123 triblock copolymer
2 was used as a supramolecular template and tetraethoxysilane (TEOS) as a silica source under near neutral
3 condition.²⁸ The hexagonally OMC was replicated from the above-synthesized SBA-15 template by using sucrose
4 as a carbon precursor. The synthesis of OMC was performed in a similar way with the synthesis of CMK-3
5 mesoporous carbon.^{29,34,35}

6
7
8
9
10
11 The NiFe_x alloy embedded OMC was performed by adding 0.1 g of OMC into nickel acetate and iron nitrate
12 solution (5 mg/mL). After stirred for 1 h and immersed for 12 h at room temperature, and evaporated at 353K, the
13 black powder was calcined at 673 K for 2 h under nitrogen flowing. The samples were hold in H₂ atmosphere at
14 723 K for 2 h. Then, the NiFe_x nanoparticles embedded OMC were obtained and labeled as Ni/OMC, NiFe/OMC,
15 and NiFe₂/OMC, respectively.
16
17
18
19

20 **Preparation of NiFe_x/OMC+Nafion+GCE and GOx+NiFe_x/OMC+Nafion+GCE**

21 Glassy carbon electrode (GCE) was grinded stepwise by using metallographic sandpaper (from 1# to 7#), then
22 polished to a mirror finish with 1.0 and 0.3 μm Al₂O₃ slurries successively, and finally washed sequentially with
23 ethanol, deionized water in ultrasonic bath, and then N₂ gas dried the electrode surface. 10mg of NiFe_x/OMC
24 catalyst and 1 mL of 0.1M PBS solution (pH 7.0) were mixed, and 25 μL of mixed catalyst was dropped on the
25 GCE by using a micro-syringe and dried at room temperature. 5 μL of the 5% Nafion-115 ® ion-crosslinked
26 polymer was mixed and dropped with droplet to the electrode surface, dried at room temperature.
27 NiFe_x/OMC+Nafion+GCE (x=0, 1, 2) was obtained.
28
29
30
31
32
33
34
35

36 GOx+NiFe_x/OMC+Nafion+GCE (x=0, 1, 2) was prepared by repeating the above process. 10 μL of GOx
37 solution (20 mg/L), 5 μL of bovine serum protein, and 5 μL of PBS (pH 6.5) solution were taken, and ultrasonic
38 mixed for 10 min, and stored at 277 K refrigerator and breed for 24 h. The mixed droplets were taken to drop on
39 the surface of the electrode. 5 μL of 5% Nafion-115 ® ionomer was plated on the electrode surface, dried at room
40 temperature.
41
42
43
44
45

46 **Results and discussion**

47 **Materials characterization**

48 Fig. 1a, 1b, and 1c show the typical TEM images of NiFe_x/OMC samples with a molar ratio for Ni:Fe of x = 0, 1,
49 2, respectively. Fig. 1d, 1e, and 1f present the size distribution of NiFe_x nanoparticles for the NiFe_x/OMC samples.
50 From Fig. 1a-1d and 1b-1e, it is shown that the average size of the Ni and NiFe nanoparticles is about 8.3 nm and
51 6.6 nm, respectively. Fig. 1c depict the typical TEM image of NiFe₂/OMC sample, indicating that the fine NiFe₂
52 nanoparticles are homogenously distributed within the pore canals of the OMC supports. Fig. 1f present the size
53 distribution of NiFe₂ nanoparticles with an average size of 4.9 nm.
54
55
56
57
58
59
60

Fig. 1.

Wide-angle XRD patterns of NiFe₂ embedded OMC samples are shown in Fig. 2a. The peaks at 44, 51, 62, and 76 degree correspond to the (111), (200), (210) and (220) planes of face-centered cubic (fcc) of NiFe₂ crystal structure.^{57,58} The XRD pattern illustrates that only pure NiFe₂ alloy nanoparticles are formed during the high temperature pyrolysis process. The typical low-angle XRD pattern of the NiFe₂/OMC composite (Fig. 2a inset) includes three well-resolved peaks assigned to (100), (110), and (200), which correspond to highly ordered 2D hexagonal *p6mm* space group, similar to that of the SBA-15 silica host. Among NiFe_x/OMC composites, NiFe₂/OMC has a high BET surface area of 1209 m² g⁻¹, a large pore volume of 1.35 cm³ g⁻¹, and an uniform pore size (4.29 nm) (shown in Fig. 2b and Fig. 2b inset). Fig. 2c shows the Raman spectrum of NiFe₂/OMC with two characteristic peaks of around 1315 cm⁻¹ (D band) and 1590 cm⁻¹ (G band), respectively. The integral intensities ratio of these two peaks (*I_D*/*I_G*) is 3.24, which shows that OMC prepared here has many edge-plane-like defective sites (EDSs) and a high electrocatalytic activity.^{34,35}

Fig. 2.

NiFe_x/OMC+Nafion+GCE detection of H₂O₂

The electrochemical impedance spectroscopy (EIS) is an effective tool for studying the interface properties of surface-modified electrodes.²⁹ In EIS, the semicircle diameter of EIS at high frequencies equals the electron transfer resistance (*R_{ct}*). The size of *R_{ct}* depends on the dielectric and its insulating properties at the electrode/electrolyte interface. The linear part at low frequencies of Warburg element (*Z_w*) relates to the kinetic and diffusion process of electrolyte. Fig. S1 exhibits the impedance spectroscopy of the Ni/OMC+Nafion+GCE and NiFe₂/OMC+Nafion+GCE as the impedance response of the system. It has been found that the diameter of the Nyquist semicircle at high frequencies decreases with increase of Fe contents because of the good distributed NiFe₂ nanoparticles, large surface area and pore volume, and suitable pore channel of NiFe₂/OMC. The *R_{ct}* of NiFe₂/OMC+Nafion+GCE is 46.3 Ω cm². Hence, the interfacial electron transfer is improved, resulting in the decrease of the electron transfer resistance.

Cyclic voltammograms (CVs) of OMC+Nafion+GCE and NiFe_x/OMC+Nafion+GCE (*x*=0, 1, 2) were detected of 1.0 mM H₂O₂ in 0.1 M PBS, shown in Fig. S2. The redox peaks of NiFe₂/OMC+Nafion+GCE is higher than that of other electrodes. It should be helpful to used for electrochemical sensor material. Fig. S3 shows the CV curves of 1.0 mM H₂O₂ on NiFe₂/OMC+Nafion+GCE at different pH values (from 5.0 to 9.0) in 0.1 M PBS. As noted in Fig. S3a, a pair of redox peaks was detected. NiFe₂/OMC electrode obtains a well-defined peaks at the redox potential for [Ni(II) and Fe(II)] to [Ni(III) and Fe(□)] (at -0.2-0 V) oxidation and an appreciable catalytic current with H₂O₂.^[37,38,41] The values of anodic peak potential (*E_{pa}*) shifts to lower negative potentials with the

1 increase of pH values. The peak potential of NiFe₂/OMC+Nafion+GCE also shows linear dependence upon the
2 solution pH in the range from 5.0 to 9.0 with the slopes of $-0.0696 \text{ V pH}^{-1}$ and $-0.0375 \text{ V pH}^{-1}$ (Fig. S3b). The
3 two values of slope are close to that given by the Nernstian equation and the electrode process, which would
4 therefore appear to be an equal proton–electron transfer.⁵⁹ The experimental results also indicate that pH value has
5 a significant influence on the values of the anodic peak current. The maximum peak currents (i_{pa}) were observed
6 at pH 7.0 (Fig. S3). Considering the current intensity in determination process of H₂O₂ and the effect of pH on the
7 reduction potential, the optimum pH value of 7.0 was employed in the following experiments. According to the
8 relationship between applied potential and H₂O₂ electrocatalytic reduction current, the optimum electrode
9 potential was selected at -0.2 V for amperometric measurements in order to obtain a good repeatability and a high
10 sensitivity. As shown in Fig. 4b, the anodic peak potential values E_{pa} moved toward a lower negative potential
11 with the increase of pH value. It shows that the higher pH values are conducive to the reduction process.⁵⁷

22 To demonstrate the efficacy of the NiFe_x/OMC+Nafion+GCE biosensor, H₂O₂ is used for amperometric
23 experiments *via* a three-electrode system. Fig. S4 displays the amperometric response plot (current vs. time, $I-t$)
24 and the response of the calibration curve (current vs. concentration) of OMC+Nafion+GCE and
25 NiFe_x/OMC+Nafion +GCE ($x=0, 1, 2$) with successive addition of 1.0 mM H₂O₂ steps to the 0.1 M PBS (pH 7.0)
26 by constant stirring at applied potential of -0.20 V . All tests involve with the detection of the redox current which
27 is associated with the reduction of peroxide at a working potential. As shown in Fig. S4a, in comparison to the
28 evident current staircases increasing achieved at NiFe_x/OMC+Nafion+GCE ($x=0, 1, 2$), a sample with pure OMC
29 in Nafion on the surface of electrode has virtually no increase in current with each successive addition of H₂O₂.
30 When the response current of NiFe_x/OMC+Nafion+GCE ($x=0, 1, 2$) reaches 95% of the steady-state currents, its
31 reaction time is 8, 6, and 5s, respectively. Among the electrodes, NiFe₂/OMC+Nafion+GCE has the highest
32 reaction rate of H₂O₂ owing to the properties of high surface area, uniform pore size and controllable structure of
33 NiFe₂/OMC. It can be demonstrated from Fig. S4b that the steady-state currents of NiFe_x/OMC+Nafion+GCE
34 increases linearly regressions for H₂O₂ reduction with the increase of H₂O₂ concentration. The linear regression
35 equations are $y_1 = 0.799 x_1 + 2.773$ ($R_1^2 = 0.99472$), $y_2 = 1.622 x_2 + 4.963$ ($R_2^2 = 0.99292$), and $y_3 = 2.327 x_3 +$
36 6.615 ($R_3^2 = 0.99574$), respectively. From the calibration curves, it can be calculated that the sensitivity of
37 NiFe₂/OMC+Nafion+GCE is higher than that of Ni/OMC+Nafion+GCE. The enhancement of sensitivity is
38 attribution to the small size of NiFe₂ nanoparticle size, which improves the ratio of active atoms with the increase
39 of the sensing efficiency of H₂O₂. By taking electron, H₂O₂ is oxidized to oxygen at the end of biochemical
40 reaction on modified electrode surface. It has been shown that a reduction reaction of H₂O₂ occurs at the
41 mediation of OMC and NiFe_x nanoparticles. (Fig. S5). Due to a catalytically active surface, NiFe_x nanoparticles
42
43
44
45
46
47
48
49
50
51
52
53
54
55
56
57
58
59
60

1 embedded OMC as a mediator, which influence charge transfer between the electrode and the analyte, can
2 promote the reduction of H₂O₂ and provide a base on the mediation for H₂O₂.^{42,58} The chemical reaction process of
3 H₂O₂ reduction is as follow:
4
5
6



8
9
10 Fig. 3a displays the dynamic response (*I-t* curve) of NiFe₂/OMC+Nafion+GCE under the optimal experimental
11 conditions with successive addition of H₂O₂ at different concentration to the 0.1 M PBS (pH 7.0) under stirring at
12 -0.2V. The current may rapidly increase after the addition of H₂O₂, and the steady-state current (95% of the
13 maximum value) is obtained within average 5 s, indicating the fast electron transfer rate between H₂O₂ and the
14 modified electrode. In addition, OMC allows rapid transport of liquid due to the porous structure, and together
15 with the extremely high surface area, which is desirable for electrochemical reactions³¹. Fig. 3b is calibration
16 curves of response current vs. H₂O₂ concentration on NiFe₂/OMC+Nafion+GCE. The linear regression equation is
17 $y = 0.30032x + 6.469$ ($R^2 = 0.99374$). The trace clearly demonstrates the fast response and high sensitivity of the
18 electrode to H₂O₂. The modified electrode has a good linear response to the concentration of H₂O₂ in the range
19 from 6.2 to 42710 μM with the sensitivity of 4.29 μA mM⁻¹ cm². The favorable amperometric signals are
20 accompanied with a low noise level, which resulted in excellent detection limit for H₂O₂. The detection limit is
21 0.24 μM when the signal to noise ratio is 3 ($S/N=3$). Therefore, NiFe₂/OMC+Nafion+GCE sensor has high
22 sensitivity, low detection limit, easy electron transition, fast response rate and wide detection scope for H₂O₂.
23 Table 1 is the comparison of the homemade sensors with the data of reported literature in linear range, sensitivity
24 and detection limit. The results show that NiFe₂/OMC+Nafion+GCE exhibits more excellent electrochemical
25 performance than that in the other recently reported electrodes (except Fe/OMC). Thus, NiFe₂/OMC which is a
26 good electrode material as an amperometric sensor for the detection of H₂O₂ has the features of low detection
27 potential, high sensitivity, and wide linear range.
28
29
30
31
32
33
34
35
36
37
38
39
40
41
42

43 **Fig. 3.**

44 **Table 1**

45
46
47 NiFe₂ alloyed nanoparticles embedded OMC can be used as not only direct electrochemical active potential
48 applications for detection of H₂O₂ but also the substrate to detect other additives such as ascorbic acid (AA),
49 sucrose, glucose, and uric acid (UA) interference. Fig. 4 shows the amperometric current curve of
50 NiFe₂/OMC+Nafion+GCE electrochemical biosensor with addition of 0.5 mM H₂O₂, sucrose, glucose, AA, and
51 UA to 0.1M PBS (pH 7.0) solution, respectively. The additives except H₂O₂ have little effect on the performance
52 of the modified electrode. This is because the cross-linked effects occur in the cation exchangers of Nafion
53 membrane can effectively prevent the distractors into the polymer film, and the electrode is not sensitive to
54
55
56
57
58
59
60

1 interference.⁶¹⁻⁶³ Therefore, NiFe₂/OMC+Nafion+GCE biosensor has a remarkable selectivity for the
2 determination of H₂O₂.
3
4

5
6 **Fig. 4.**

7 The current response of NiFe₂/OMC+Nafion+GCE electrochemical biosensor mainly remained unchanged in
8 0.1 M PBS (pH 7.0) +0.5 mM H₂O₂ through consecutive scanning of 50 circles, which can be seen in the CV. The
9 relative standard deviation (RSD) is 3.6% after five times in the same test, suggesting the reliable fabrication
10 procedure of the sensor, thereby allowing reproducible electroanalysis responses to be obtained with different
11 composition electrodes constructed in the same manner. It shows that the electrochemical biosensor electrode has
12 good reproducibility. Long-term stability of electrochemical biosensor is one of the most importance features to
13 meet the application. In order to evaluate its stability, NiFe₂/OMC+Nafion+GCE was stored in a solution of 0.1 M
14 PBS (pH 7.0) in air ambient conditions for 4 weeks. And every other week, its current response was obtained in
15 the same process. The result shows that the current response has little change. Compared with the initial value of
16 biosensor, the sensitivity only falls by 5% after 4 weeks, which shows a strong binding between the mediator and
17 the matrix. The mediator of NiFe₂/OMC+Nafion prevents the leaching contaminants by the electron transfer
18 reaction. Therefore, the application of the mediator provides both mechanical and chemical stability to the
19 electrode. It means that NiFe₂/OMC+Nafion+GCE has good activity and stability for H₂O₂.
20
21
22
23
24
25
26
27
28
29
30
31

32 **GOx+NiFe_x/OMC+Nafion+GCE detection of glucose**

33 The Nyquist diagrams of GOx+Ni/OMC+Nafion+GCE and GOx+NiFe₂/OMC+Nafion+GCE are recorded at
34 the oxidation peak potential for the concentrations of 1.0 mM glucose in 0.1 M PBS (pH 6.5), shown in Fig. S6. In
35 the case of above electrode materials, the diameter of its semicircle at high frequencies is related to the resistance
36 (R_{ct}) of the charge transfer reaction and the electronic resistance of the modified film. By analyzing the linear part
37 at low frequency region, it can be observed that the process turns from a semi-infinite diffusion to a finite
38 diffusion on the surfaces of GOx+Ni/OMC+Nafion+GCE and GOx+NiFe₂/OMC+Nafion +GCE. Compared with
39 the diameter of the semicircle present in the high frequency region on GOx+Ni/OMC+ Nafion+GCE, a lower
40 resistance R_{ct} can be observed for GOx+NiFe₂/OMC+Nafion+GCE of 73.4 Ω cm². This phenomenon indicates
41 that GOx immobilized on OMC with the NiFe₂ nanoparticles can promote the charge transfer rate.
42
43
44
45
46
47
48
49

50 Fig. S7 shows cyclic voltammograms of GOx+OMC+Nafion+GCE and GOx+NiFe_x/OMC+Nafion+GCE ($x=0,$
51 1, 2), which detect of 1.0 mM glucose in 0.1 M PBS. GOx+NiFe₂/OMC+Nafion+GCE has the highest redox
52 peaks for biosensor material. The CVs and the relation plots of potential E_{pa} vs. current I_{pa} are tested in a solution
53 of 1.0 mM glucose and 0.1 M PBS at different pH values (6.0 ~8.0) of GOx+NiFe₂/OMC+Nafion+GCE (shown
54 in Fig. S8a). A pair of oxidation and reduction peaks of each electrode was found between -0.5 and 0.2 V, and the
55
56
57
58
59
60

current peak was smaller than that of NiFe₂/OMC+Nafion+GCE. In addition, the redox peaks shifted toward the positive potential because of the glucose oxidation-reduction reaction on GOx. Fig. S8b shows the linear relationship between potentials and pH values. The slope of line is -0.0604 V pH⁻¹, which is close to that reported in the literature (the GOx (FADH₂) conversion reaction theoretical value of -59 mV pH⁻¹). It illustrates that this is reaction process of a two-electron, two-proton (2e, 2H).⁶³⁻⁶⁵ By using the pH value of 6.5, the current value *I*_{pa} is up to the maximum. Accordingly, a solution pH value of 6.5 is used in subsequent experiments. It should be noted that 0.2 V is selected because such an applied potential would be beneficial to decrease the background current and minimize the responses of common interference species.

Due to its excellent analytical performance for the detection of H₂O₂, the biorecognition species such as enzymes immobilized NiFe_x/OMC+Nafion+GCE is further explored as platform for the construction of biosensors. The biosensors were prepared by anchoring GOx on the NiFe_x/OMC *via* cross linking with Nafion. Typically, the current response of GOx+NiFe_x/OMC+Nafion+GCE is in accord with the electrocatalytic reaction of glucose oxidase molecules in successive addition of 0.5 mM glucose to 0.1 M PBS (pH 6.5) solution and continuously stirred at 0.2 V (shown in Fig. S9a). Glucose biosensor was accomplished in the same electroanalytical procedures as in the experiments of H₂O₂. The intermediate product of H₂O₂ can directly be generated by the electrooxidation reaction occurring on the enzymatic reaction of GOx+NiFe_x/OMC+Nafion+GCE for glucose, which is proportional to the glucose concentration. Fig. S9b shows that the linear calibration curves of regression equations of GOx+NiFe_x/OMC+Nafion+GCE (*x*=0, 1, 2) are $y_4 = -0.06521x_4 - 0.2325$ ($R_4^2 = 0.99286$), $y_5 = -0.13435x_5 - 0.269$ ($R_5^2 = 0.99426$), and $y_6 = -0.32515x_6 - 0.5575$ ($R_6^2 = 0.99613$), respectively. It can be calculated that GOx+NiFe₂/OMC+Nafion +GCE has not only a high sensitivity, but also a fast response to glucose.

In order to assess the biological activity of GOx immobilized on the surface of the biosensor, the Michaelis-Menten constant (*K*'_{*M*}) is determined by the current changes by using the Lineweaver-Burk-type formula (shown in formula (1)).⁶⁶

$$\frac{1}{i_{ss}} = \left(\frac{K'_M}{i_{max}} \right) \left(\frac{1}{C} \right) \left(\frac{1}{i_{max}} \right) \quad (1)$$

where *i*_{ss} is the steady-state current of the given concentration (*C*), *i*_{max} is the maximum testing current when the analyte is saturated. The effective Michaelis-Menten constant (*K*'_{*M*}) of GOx+NiFe₂/OMC+Nafion+GCE biosensor is 3.18 mM calculated from Fig. 5a, which is inferior to CNT-based biosensor of 8.2 mM⁶⁷, glucose at the GOx/Pt/Fe₃O₄-MWCNTs/CS of 9 mM⁵², the glucose sensor (GOx-GCE) fabricated by sol-gel of 22 and 23 mM^{65,68}, and GOx in a glucose sensor of 15.7 mM⁶⁹. Assumed that the rate of the enzymatic reaction is controlled by the quality of the transmission⁶⁹, then, the lower Michaelis-Menten constant is related to the sensitivity and

1 detection limit, and it can be considered that the GOx+NiFe₂/OMC+Nafion+GCE generates a unique
2 microenvironment of enzymic biosensor. Thus, the prepared electrode of GOx+NiFe₂/OMC+Nafion+GCE
3 exhibits high affinity for glucose, and GOx immobilized on OMC maintains a high enzymic activity. It can be
4 seen from Fig. 5b that the linear regression equation of low concentration is $y' = -0.49014x' - 0.12929$ ($R^2 = 0.99715$).
5 Under the low concentration of glucose, NiFe₂/OMC+Nafion+GCE immobilized by active GOx has a high
6 detection sensitivity ($6.90 \mu\text{A mM}^{-1} \text{cm}^{-2}$), a wide linear detection range (from 48.6 to 12500 μM), and a low
7 detection limit ($2.7 \mu\text{M}$ ($S/N = 3$)). Compared with pure OMC, NiFe_x nanoparticles embedded OMC is ideal
8 promote body for electron transfer, particularly in the low concentration levels of additives. The lower noise and
9 higher detection sensitivity can be obtained by the biosensor. In addition, GOx+NiFe₂/OMC+Nafion modified
10 electrode responses to glucose more quickly, whose current reaches to 95% of steady-state current within 6s.
11 Compared with glucose electrochemical biosensor recently reported (Table 2), the NiFe₂ nanoparticles embedded
12 OMC has a higher biocatalytic performance, and the self-control biosensor for glucose has a more sensitive
13 response and a lower detection limit.
14
15
16
17
18
19
20
21
22
23
24
25

26 **Fig. 5**

27 **Table 2**

28
29
30 The possible interferences at the modified electrode have also been investigated and the results are shown in
31 Fig. 6. Selectivity is an important assessment indicator of the application of electrochemical biosensor. 0.5 mM of
32 glucose, AA, UA, and sucrose solution are added in 0.1 M PBS (pH 6.5) for observing current response. The
33 results show that AA solution significantly enhances the current response signals, while the rests (UA, sucrose)
34 have not been found any obvious current response signal for interference. Therefore, GOx+NiFe₂/OMC+Nafion
35 +GCE electrochemical biosensor try to minimize the contact with AA in the practical application.
36
37
38
39
40
41

42 **Fig. 6.**

43 The redox reaction drawing of glucose on the enzymic electrode is shown in Fig. 7. NiFe_x nanoparticles
44 embedded OMC can be used as electron transfer relaying media (MED or M) for shortening the electron transfer
45 distance between the center of enzyme redox and the electrode surface, which create synergy with OMC for
46 accelerating the electron transfer rate and improving of electrocatalytic performance. Furthermore, due to a high
47 specific surface area, OMC composite materials have a great adsorption capacity of activity materials and increase
48 the contact chance with glucose. GOx+NiFe₂/OMC+Nafion +GCE could be used to detect of glucose based on the
49 consumption of O₂ with the oxidation of glucose catalyzed by GOx. The by product of glucose oxidation reaction
50 is H₂O₂ (Fig. 7b). The reduction effect of NiFe_x nanoparticles on H₂O₂ is very strong, which greatly enhances the
51 electrocatalytic properties and electrical conductivity coupled with the synergistic effect, and can provide an
52
53
54
55
56
57
58
59
60

1 amount of channels to promote the electron transfer between the NiFe_x/OMC and the electrode. And it finally
2 results in enhancement of the effect of the electric sensing. If the glucose oxidase as redox centers were deep in
3 the protein shell, it is difficult to achieve the reaction of direct electron transfer in the normal electrode. This
4 challenge can be overcome while the glucose oxidase is immobilized on matrix such as CNT, OMC, and graphene.
5
6
7
8
9
10
11
12
13
14
15
16
17
18
19
20
21
22
23
24
25
26
27
28
29
30
31
32
33
34
35
36
37
38
39
40
41
42
43
44
45
46
47
48
49
50
51
52
53
54
55
56
57
58
59
60

71,72 A good electrical activity and large specific surface area of NiFe_x nanoparticles embedded OMC after the immobilization GOx can be used to effectively promote the electron transfer between the enzyme and the electrode. While a higher amount of NiFe_x/OMC is obtained, the glucose oxidase molecules exhibit the behavior of direct electron transfer.^{5,63,73}

Fig. 7.

Additionally, the current response of the biosensor has unchanged after 50 laps continuous cyclic voltammetry in 0.1 M PBS (pH 6.5) and 0.5 mM glucose solution, showing its high reproducibility. The relative standard deviation (RSD) is 5.3 % after the same five tests. The electrodes are not poisoned by the oxidation products and can be used repeatedly for the detection of glucose. In order to evaluate the stability of glucose biosensor, we made the investigation through the amperometric response to 0.5 mM glucose in 0.1M PBS at intervals over several days, and then stored the electrode in a solution of 0.1 M PBS (pH 6.5) at 277 K. After 4 weeks, the current response was essentially constant after the same scan. Compared with the initial value of the sensitivity of the sensor, the sensitivity dropped only 7%, showing the long-term stability and good biocompatibility of GOx+NiFe₂/OMC+Nafion+GCE for glucose, shown in Fig. 8. It means that the enzymic glucose biosensor possesses a good superiority in terms of biological activity, sensitivity, selectivity and stability.

Fig. 8

Conclusions

NiFe_x/OMC nanocomposites have been successfully fabricated by wet impregnation and hydrogen reduction process. The nanocomposites of well-dispersion NiFe_x nanoparticles embedded OMC show a large surface area, suitable mesoporous channels, and many edge-plane-like defective sites. NiFe_x/OMC+Nafion+GCE and GOx+NiFe_x/OMC+Nafion+GCE electrochemical biosensors were composed of NiFe_x/OMC, GOx, and Nafion on GCE, respectively, and detected in PBS. NiFe₂/OMC used as electrochemical biosensor electrode materials exhibit a better quasi-reversible reaction and low electron transfer resistance (R_{ct}). When the different concentration of H₂O₂ is added to 0.1 M PBS (pH 7.0), NiFe₂/OMC+Nafion+GCE shows excellent electrochemical reduction activity of H₂O₂, which exhibits a high sensitivity of 4.29 $\mu\text{A mM}^{-1} \text{cm}^{-2}$, wide detection range from 6.2 to 42710 μM and low detection limit of 0.24 μM ($S/N=3$). Furthermore, GOx+NiFe₂/OMC+Nafion

+GCE demonstrates great electrochemical oxidation effects of glucose. The glucose biosensor showed good analytical characteristics such as a wide detection range from 48.6 to 12500 μM with high sensitivity of 6.9 $\mu\text{A mM}^{-1} \text{cm}^{-2}$, low detection limit of 2.7 μM ($S/N=3$) and low Michaelis–Menten constant ($K_M=3.18 \text{ mM}$). The about results were attributed to the direct electron transfer process between the mediator (or GOx) and electrodes because of the large specific area of OMC and the catalytic activity of NiFe_2 nanoparticles. The two kinds of $\text{NiFe}_2/\text{OMC}+\text{Nafion}+\text{GCE}$ and $\text{GOx}+\text{NiFe}_2/\text{OMC}+\text{Nafion}+\text{GCE}$ display high sensitivity, good stability and acceptable reproducibility.

Acknowledgments

We acknowledge support from the National Natural Science Funds for Distinguished Young Scholars (51025211), National Nature Science Foundation of China (Nos.50872071 and 50972079), the Shandong Natural Science Fund for Distinguished Young Scholars (JQ200915), the Nature Science Foundation of Shandong Province (Y2007F03 and Y2008F26), the Foundation of Outstanding Young Scientists in Shandong Province (No. 2006BS04030), the Tai Shan Scholar Foundation of Shandong Province, and the Gong Guan Foundation of Shandong Province (2008GG10003019).

Note and references

- 1 J. C. Claussen, A. D. Franklin, A. UlHaque, D. M. Porterfield and T. S. Fisher, *ACS nano*, 2009, **3**, 37.
- 2 T. G. Drummond, *Nat. Biotechnol.*, 2003, **21**, 1192.
- 3 S. Chen, R. Yuan, Y. Chai and F. Hu, *Microchimica. Acta*, 2013, **180**, 15.
- 4 X. H. Kang, Z. B. Mai, X. Y. Zou, P. X. Cai and J. Y. Mo, *Anal. Biochem.*, 2007, **369**, 71.
- 5 J. Luo, H. Zhang, S. Jiang, J. Jiang and X. Liu, *Microchimica. Acta*, 2012, **177**, 485.
- 6 Y. F. Zheng, G. W. Xu, D. Y. Liu, J. H. Xiong, P. D. Zhang, C. Zhang, Q. Yang and S. Lv, *Electrophoresis*, 2002, **23**, 4104.
- 7 S. Hanaoka, J. M. Lin and M. Yamada, *Anal. Chim. Acta*, 2001, **426**, 57.
- 8 A. Lupu, P. Lisboa, A. Valsesia, P. Colpo and F. Rossi, *Sensors Actuators B: Chem.*, 2009, **137**, 56.
- 9 J. Xuan, L. P. Jiang and J. J. Zhu, *Chin. J. Anal. Chem.*, 2010, **38**, 513.
- 10 G. Wang, X. He, L. Wang, A. Gu, Y. Huang, B. Fang, B. Geng and X. Zhang, *Microchimica. Acta*, 2013, **180**, 161.
- 11 B. J. Wang, S. Q. Gu, Y. P. Ding, Y. L. Chu, Z. Zhang, X. Ba, Q. L. Zhang and X. X. Li, *Analyst*, 2012, **138**, 362.
- 12 Y. F. Yang and S. L. Mu, *J. Electroanal. Chem.*, 1997, **432**, 71.
- 13 L. D. Zhu, C. Y. Tian, D. X. Zhu and R. L. Yang, *Electroanalysis*, 2008, **20**, 1128.
- 14 N. Pena, G. Ruiz, J. Reviejo and J. M. Pingarron, *Anal. Chem.*, 2001, **73**, 1190.
- 15 D. Z. Sun, L. D. Zhu and G. Y. Zhu, *Anal. Chim. Acta*, 2006, **564**, 243.
- 16 A. Schulte and R. H. Chow, *Anal. Chem.*, 1996, **68**, 3054.
- 17 H. X. Luo, Z. J. Shi, N. Q. Li, Z. N. Gu and Q. K. Zhuang, *Anal. Chem.*, 2001, **73**, 915.
- 18 J. Wang, G. Chen, M. P. Chatrathi and M. Musameh, *Anal. Chem.*, 2004, **76**, 298.
- 19 R. Ryoo, S. H. Joo, S. M. Kruk and S. Jun, *J. Phys. Chem. B.*, 1999, **103**, 7743.
- 20 M. Hartmann, *Chemical Materials*, 2005, **17**, 4577.
- 21 M. Zhou, J. Ding, L. P. Guo and Q. K. Shang, *Anal. Chem.*, 2007, **79**, 5328.
- 22 M. Zhou, L. P. Guo, F. Y. Lin and H. X. Liu, *Anal. Chim. Acta*, 2007, **587**, 124.
- 23 L. D. Zhu, C. Y. Tian, D. X. Zhu, X. Y. Jiang and R. L. Yang, *Electroanalysis*, 2008, **20**, 2518.
- 24 J. Bai, X. X. Bo, B. Qi and L. P. Guo, *Electroanalysis*, 2010, **22**, 1750.
- 25 J. Bai, B. Qi, C. Ndamanisha and L. P. Guo, *Microporous Mesoporous Mater.*, 2009, **119**, 193.
- 26 X. Bo, J. Bai, L. Wang and L. Guo, *Talanta*, 2010, **81**, 339.
- 27 L. Liu, L. P. Guo, X. J. Bo, J. Bai and X. J. Cui, *Anal. Chim. Acta.*, 2010, **673**, 88.
- 28 A. Vinu, M. Miyahara and K. Ariga, *J. Phys. Chem. B*, 2005, **109**, 6436.
- 29 H. Zhou, S. Zhu, M. Hibino and I. Honma, *J. Power Sources*, 2003, **122**, 219.
- 30 C. D. Liang and S. Dai, *J. Am. Chem. Soc.*, 2006, **128**, 5316.
- 31 Y. F. Zhang, X. J. Bo, A. Nsabimana, C. Luhana, G. Wang, H. Wang, M. Li and L. P. Guo, *Biosens. Bioelectron.*, 2014, **53**, 250.
- 32 N. Jia, Z. Wang, G. Yang, H. Shen and L. Zhu, *Electrochem. Commun.*, 2007, **9**, 233.
- 33 M. Zhou, L. Shang, B. L. Li, L. J. Huang and S. J. Dong, *Electrochem. Commun.*, 2008, **10**, 859.
- 34 M. R. Guascito, E. Filippo, C. Malitesta, D. Manno, A. Serra and A. Turco, *Biosens. Bioelectron.*, 2008, **24**, 1063.
- 35 X. Y. Jiang, Y. H. Wu, X. Y. Mao, X. J. Cui and L. D. Zhu, *Sens. Actuators B Chem.*, 2011, **153**, 158.
- 36 H. Rajabzade, P. Daneshgar, E. Tazikeh and R. Z. Mehrabian, *Journal of Chemistry*, 2012, **9**, 2540.
- 37 C. M. Welch, C. E. Banks, A. O. Simm and R. G. Compton, *Anal. Bioanal. Chem.*, 2005, **382**, 12.
- 38 I. Danaee, M. Jafarian, F. Forouzandeh, F. Gobal and M. G. Mahjani, *Electrochim. Acta*, 2008, **53**, 6602.
- 39 L. M. Lu, L. Zhang, F. L. Qu, H. X. Lu, X. B. Zhang, Z. S. Wu, S. Y. Huan, Q. A. Wang, G. L. Shen and R. Q. Yu, *Biosens. Bioelectron.*, 2009, **25**,

218.

- 40 X. M. Miao, R. Yuan, Y. Q. Chai, Y. T. Shi and Y. Y. Yuan, *J. Electroanal. Chem.*, 2008, **612**, 157.
- 41 W. Z. Jia, M. Guo, Z. Zheng, T. Yu, E. G. Rodriguez, Y. Wang and Y. Lei, *J. Electroanal. Chem.*, 2009, **625**, 27.
- 42 J. Yu, D. Yu, T. Zhao and B. Zeng, *Talanta*, 2008, **74**, 1586.
- 43 J. C. Ndamaniha, Y. Hou, J. Bai and L. P. Guo, *Electrochim. Acta*, 2009, **54**, 3935.
- 44 L. Meng, J. Jin, G. Yang, T. Lu, H. Zhang and C. Cai, *Anal. Chem.*, 2009, **81**, 7271.
- 45 K. J. Chen, K. Chandrasekara Pillai, J. Ricka, C. J. Pan, S. H. Wang, C. C. Liu and B. J. Hwang, *Biosens. Bioelectron.*, 2012, **33**, 120.
- 46 N. A. Grace and K. Pandian, *Electrochem. Commun.*, 2006, **8**, 1340.
- 47 J. Luo, P. N. Njoki, Y. Lin, D. Mott, L. Y. Wang and Z. Jian, *Langmuir : the ACS journal of surfaces and colloids*, 2006, **22**, 2892.
- 48 C. C. Yang, A. S. Kumar, M. C. Kuo, S. H. Chien and J. M. Zen, *Anal. Chim. Acta*, 2005, 554, 66.
- 49 S. Devarajan, P. Bera and S. Sampath, *J. Colloid. Interface Sci.*, 2005, **290**, 117.
- 50 Y. Li, J. J. Zhang, J. Xuan, L. P. Jiang and J. J. Zhu, *Electrochem. Commun.*, 2010, **12**, 777.
- 51 X. Cui, Z. Li, Y. Yang, W. Zhang and Q. Wang, *Electroanalysis*, 2008, **20**, 970.
- 52 C. M. Welch and R. G. Compton, *Anal. Bioanal. Chem.*, 2006, **384**, 601.
- 53 X. Kang, Z. Mai, X. Zou, P. Cai and J. Mo, *Anal. Biochem.*, 2007, **363**, 143.
- 54 U. Yogeswaran, S. Thiagarajan and S. M. Chen, *Anal. Biochem.*, 2007, **365**, 122.
- 55 P. C. Pandey and A. K. Pandey, *BioNanoScience*, 2012, **2**, 127.
- 56 H. B. Noh, K. S. Lee, P. Chandra, M. S. Won and Y. B. Shim, *Electrochim. Acta*, 2012, **61**, 36.
- 57 K. V. P. M. Shafi, A. Gedanken, R. B. Goldfarb, I. Felner, *J. Appl. Phys.*, 1997, 81 (10), 6901-6905.
- 58 S. H. Kima, H.J. Sohna, Y. C. Jooa, Y. W. Kima, T. H. Yimb, H. Y. Leeb, T. Kang, *Surf. Coat Tech.*, 2005, 199, 43-48.
- 59 Z. H. Wen, S. Q. Ci and J. H. Li, *J. Phys. Chem. C*, 2009, **113**, 13482.
- 60 S. A. G. Evans, J. M. Elliott, L. M. Andrews, P. N. Bartlett, P. J. Doyle and G. Denuault, *Anal. Chem.*, 2002, **74**, 1322.
- 61 G. F. Wang, Y. Wei, W. Zhang, X. J. Zhang, B. Fang and L. Wang, *Microchimica Acta*, 2009, **168**, 87.
- 62 Y. Liu, M. Wang, F. Zhao, Z. Xu and S. Dong, *Biosens. Bioelectron.*, 2005, **21**, 984.
- 63 S. J. Bao, C. M. Li, J. F. Zang, X. Q. Cui, Y. Qiao and J. Guo, *Adv. Funct. Mater.*, 2008, **18**, 591.
- 64 S. Deng, G. Jian, J. Lei, Z. Hu and H. Ju, *Biosens. Bioelectron.*, 2009, **25**, 373.
- 65 S. Q. Liu and H. X. Ju, *Biosens. Bioelectron.*, 2003, **19**, 177.
- 66 R. A. Kamin and G. S. Wilson, *Anal. Chem.*, 1980, **52**, 1198.
- 67 B. Q. Wang, B. Li, Q. Deng and S. J. Dong, *Anal. Chem.*, 1998, **70**, 3170.
- 68 M. C. Rodriguez and G. A. Rivas, *Electroanalysis*, 1999, **11**, 558.
- 69 J. J. Xu, Chen, H. Y., *Anal. Chim. Acta*, 2000, **423**, 101.
- 70 L. Wang, J. Bai, X. Bo, X. Zhang and L. Guo, *Talanta*, 2011, **83**, 1386-1391.
- 71 Y. D. Zhao, W. D. Zhang, H. Chen and Q. M. Luo, *Anal. Sci.*, 2002, **18**, 939.
- 72 G. E. Anthony, C. H. Lei and R. H. Baughman, *Nanotechnol.*, 2002, **13**, 559.
- 73 S. Dönmez, F. Arslan, N. Sari, N. K. Yetim and H. Arslan, *Biosens. Bioelectron.*, 2014, **54**, 146.

Fig. 1 TEM images and the particle size distribution of NiFe_x/OMC, (a) Ni/OMC, (b) NiFe/OMC, (c)

1 NiFe₂/OMC.
2
3
4

5 **Fig. 2** (a) The wide angle X-ray diffraction (XRD) pattern of NiFe₂/OMC, inset: low angle XRD of NiFe₂/OMC,
6 (b) N₂ adsorption–desorption curves (open symbols: adsorption; closed symbols: desorption), inset: the pore size
7 distribution plot for NiFe₂/OMC sample, (c) Raman spectra for the NiFe₂/OMC composite at room-temperature
8
9

10
11 **Fig. 3** (a) *I-t* response curve for successive addition of different H₂O₂ concentrations at NiFe₂/OMC+Nafion
12 +GCE, measured in 0.1M PBS (pH 7) solution at –0.20 V in N₂ saturated, rotation speed: 400 rpm, (b) calibration
13 curves of response current vs. H₂O₂ concentration.
14
15
16

17
18 **Fig. 4** Amperometric response of 0.5 mM H₂O₂, sucrose, UA, AA, and glucose at NiFe₂/OMC+Nafion+GCE in
19 N₂ saturated 0.1M PBS (pH 7), applied potential: –0.2 V, rotation speed: 400 rpm.
20
21
22

23
24 **Fig. 5** (a) *I-t* response curve for successive addition of different glucose concentrations at GOx+NiFe₂/OMC
25 +Nafion+GCE, measured in 0.1M PBS pH 6.5 solution at 0.20 V, rotation speed: 400 rpm, (b) calibration curves
26 of response current vs. glucose concentration at low concentration and at high concentration.
27
28
29

30
31
32 **Fig. 6** Amperometric response of 0.5 mM glucose, sucrose, UA, AA at GOx+NiFe₂/OMC+Nafion+GCE in N₂
33 saturated 0.1M PBS (pH 6.5), applied potential: 0.2 V, rotation speed: 400 rpm.
34
35
36

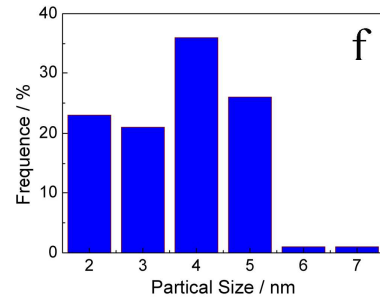
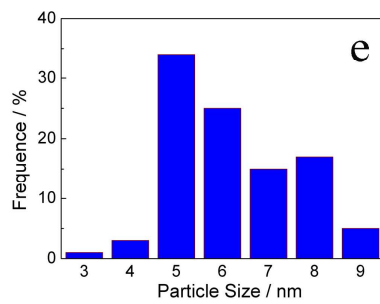
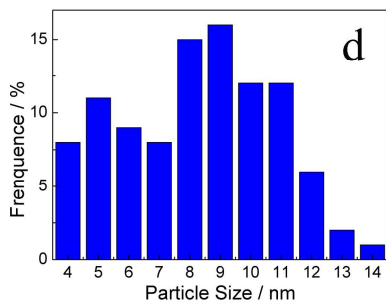
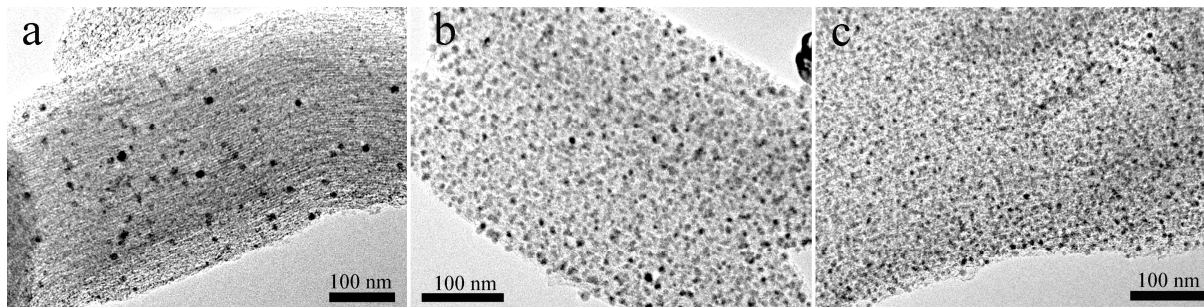
37 **Fig. 7** (a) The redox reaction drawing of glucose biosensors-mediated on enzyme, (b) the reaction process
38 between glucose and GOx+NiFe₂/OMC+Nafion+GCE.
39
40
41

42
43 **Fig. 8** Stability of the amperometric response of GOx+NiFe₂/OMC+Nafion+GCE of 0.5 mM glucose in 0.1 M
44 PBS solution for 4 weeks.
45
46

47
48 Table 1 Comparison of the performance of various hydrogen peroxide sensors
49
50

51 Table 2 Comparison of the performance of various glucose sensors
52
53
54
55
56
57
58
59
60

Fig. 1



1
2
3
4
5
6
7
8
9
10
11
12
13
14
15
16
17
18
19
20
21
22
23
24
25
26
27
28
29
30
31
32
33
34
35
36
37
38
39
40
41
42
43
44
45
46
47
48
49
50
51
52
53
54
55
56
57
58
59
60

Fig. 2

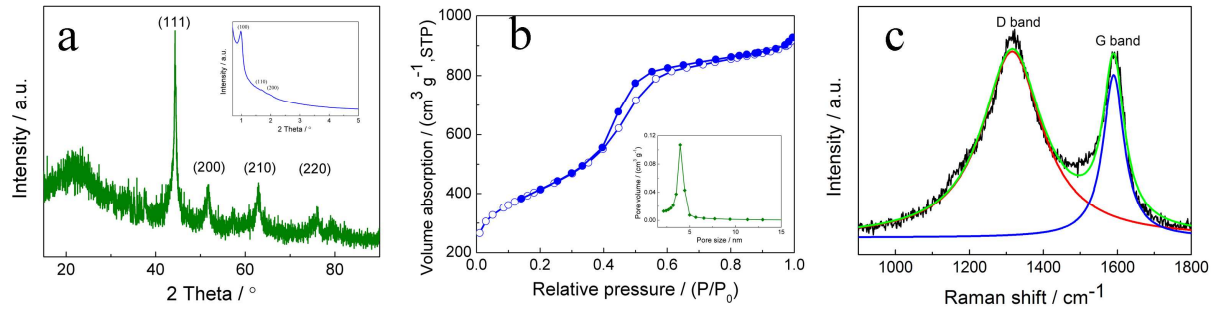
1
2
3
4
5
6
7
8
9
10
11
12
13
14
15
16
17
18
19
20
21
22
23
24
25
26
27
28
29
30
31
32
33
34
35
36
37
38
39
40
41
42
43
44
45
46
47
48
49
50
51
52
53
54
55
56
57
58
59
60

Fig. 3

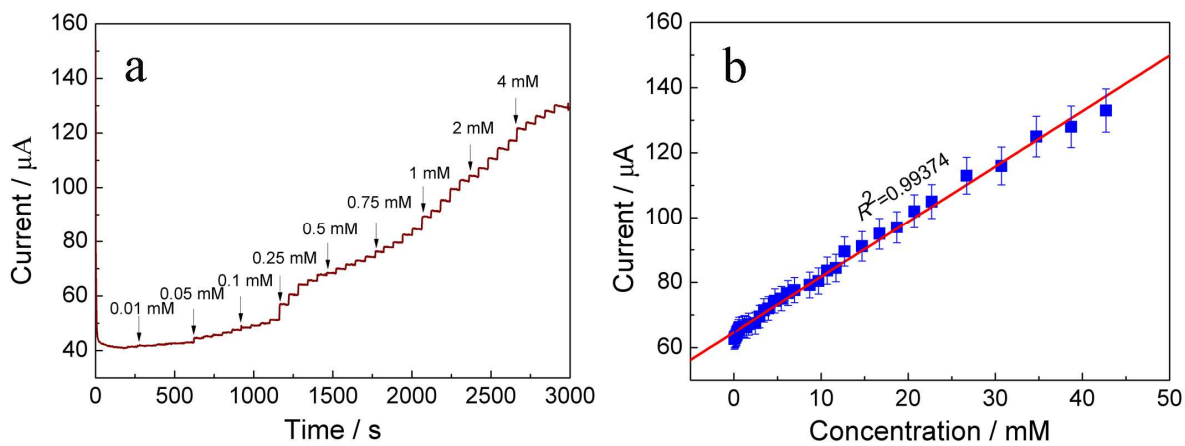
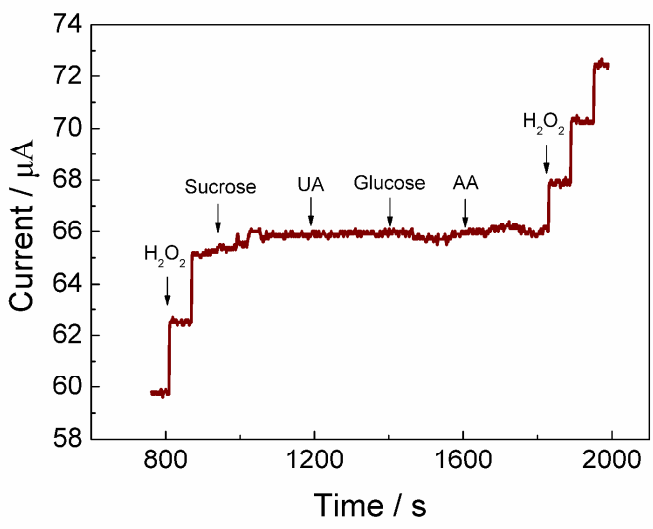
1
2
3
4
5
6
7
8
9
10
11
12
13
14
15
16
17
18
19
20
21
22
23
24
25
26
27
28
29
30
31
32
33
34
35
36
37
38
39
40
41
42
43
44
45
46
47
48
49
50
51
52
53
54
55
56
57
58
59
60

Fig.4



1
2
3
4
5
6
7
8
9
10
11
12
13
14
15
16
17
18
19
20
21
22
23
24
25
26
27
28
29
30
31
32
33
34
35
36
37
38
39
40
41
42
43
44
45
46
47
48
49
50
51
52
53
54
55
56
57
58
59
60

Fig. 5

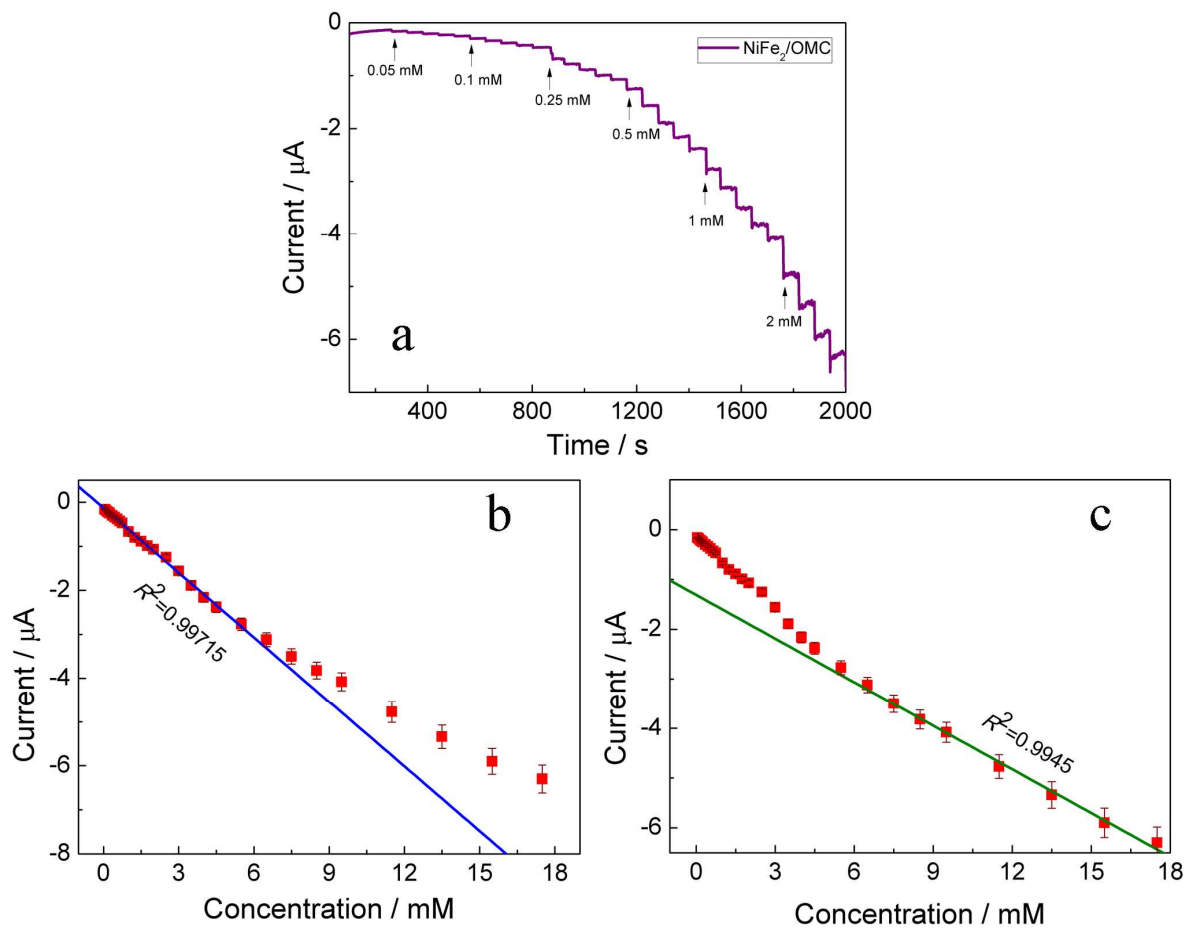
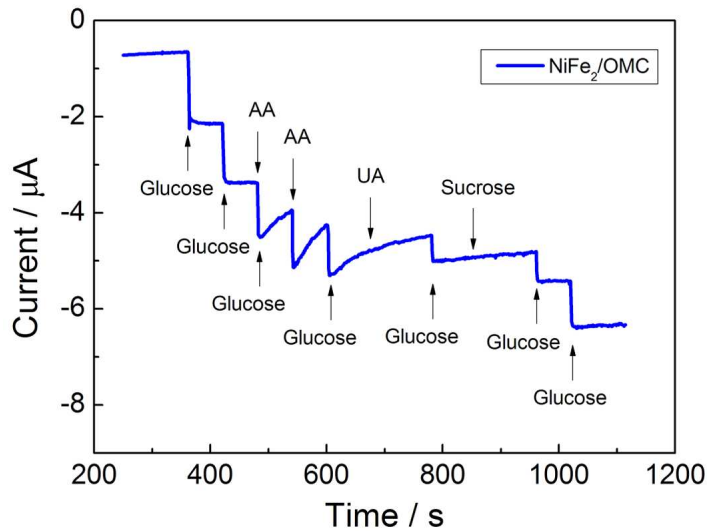
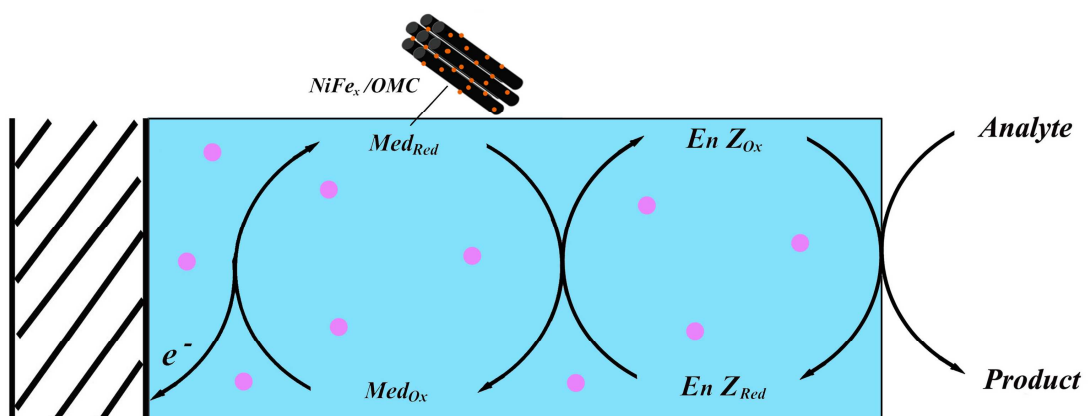


Fig. 6



1
2
3
4
5
6
7
8
9
10
11
12
13
14
15
16
17
18
19
20
21
22
23
24
25
26
27
28
29
30
31
32
33
34
35
36
37
38
39
40
41
42
43
44
45
46
47
48
49
50
51
52
53
54
55
56
57
58
59
60

Fig. 7

1
2
3
4
5
6
7
8
9
10
11
12
13
14
15
16
17
18
19
20
21
22
23
24
25
26
27
28
29
30
31
32
33
34
35
36
37
38
39
40
41
42
43
44
45
46
47
48
49
50
51
52
53
54
55
56
57
58
59
60

1
2
3
4
5
6
7
8
9
10
11
12
13
14
15
16
17
18
19
20
21
22
23
24
25
26
27
28
29
30
31
32
33
34
35
36
37
38
39
40
41
42
43
44
45
46
47
48
49
50
51
52
53
54
55
56
57
58
59
60

Fig. 8

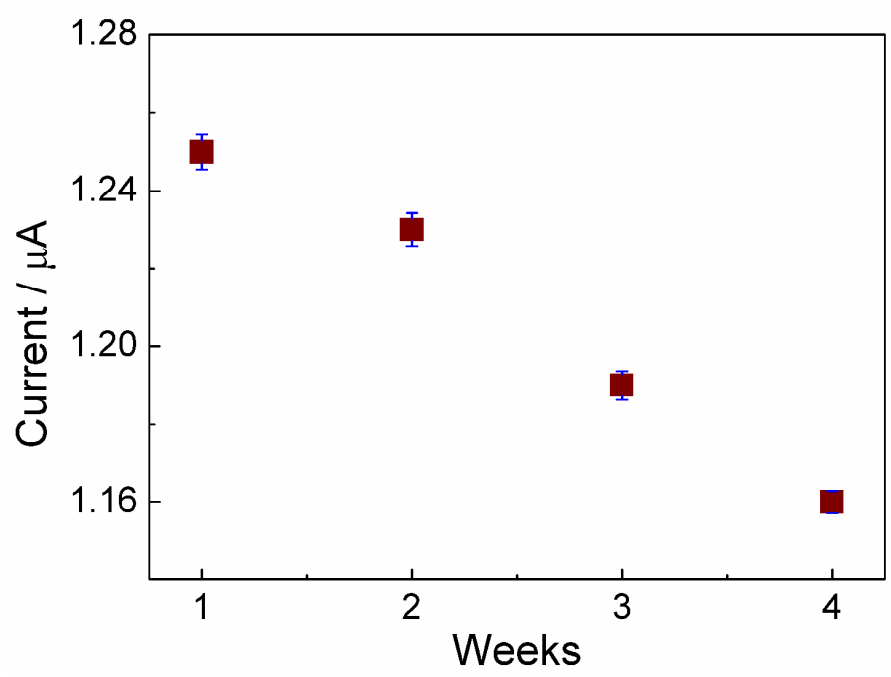


Table 1

Electrode materials	Linear range	Sensitivity	Detection limit	Ref.
	/ μM	/ $(\mu\text{A mM}^{-1} \text{ cm}^{-2})$	/ μM	
NiFe ₂ /OMC	6.2-42710	4.29	0.24	This work
Fe/OMC	7.0-4000	8.4	0.036	42
Pt/CNT	5.0-25000	1.4	1.5	59
Au/CNT	0.02-300	0.11	0.4	35
P2Mo18/OMC	5.34-24000	2.8	1.78	21
Mesoporous Pt	20-40000	2.8	4.5	60
OMC	10-1000	1.95	2.23	12

Table 2

Electrode materials	Linear range / μM	Sensitivity / $(\mu\text{A mM}^{-1} \text{cm}^{-2})$	Detection limit / μM	Ref.
GO _x +NiFe ₂ /OMC	48.6-12500	6.90	2.7	This work
GO _x /Pt/OMC	40-12200	1.79	10	41
GO _x /OMC	53-15000	0.018	72	12
GO _x +Pt/CNT	160-11500	1.28	55	59
GO _x /OMC/Au	50-20000	4.34	12	70